Influence of mechanical surface treatments on the high cycle fatigue performance of TIMETAL 54M

K. Zay[a,*], E. Maawad[a], H.-G. Brokmeier[a,b], L. Wagner[a] and Ch. Genzel[c]

[a] Clausthal University of Technology, Institute of Materials Science and Engineering, Clausthal-Zellerfeld D-38678, Germany.

[b] GKSS Research Center, Geesthacht D-21502, Germany

[c] Helmholtz-Zentrum Berlin (BESSY-II), Berlin, Germany

Abstract

TIMETAL 54M (in the following Ti-54M) is a newly developed (α+β) titanium alloy with nominal composition Ti-5Al-4V-0.6Mo-0.4Fe. The alloy can provide a cost benefit over Ti-6Al-4V due to improved machinability and formability. These attractive properties might be a driving force for replacing Ti-6Al-4V in many aircraft as well as biomedical applications. Since HCF performance is one of the most important requirements for these applications, it is essential to improve this property by microstructural optimization and by mechanical surface treatments such as shot peening or ball burnishing. The latter improvement is mainly the result of induced near-surface severe plastic deformation which results in work-hardening and the generation of compressive residual stresses that retard fatigue crack propagation. The main aim of the present study was to investigate the potential fatigue life improvements in Ti-54M due to shot peening and ball-burnishing. The process-induced residual stresses and stress-depth profiles were determined by energy-dispersive X-ray diffraction (ED) of synchrotron radiation with the beam energy of 10-80 keV. Results on Ti-54M and Ti-6Al-4V will be compared and correlated with the mean stress and environmental sensitivities of the fatigue strengths in the various microstructures.

* Corresponding author: Tel.: +49-05323-72-2699; fax: +49-05323-72-2766.
E-mail address: zay.khaung@tu-clausthal.de
Postal address: IWW, Agricolastr. 6, 38678 Clausthal-Zellerfeld, Germany.

Keywords:

TIMETAL 54M; mechanical surface treatments; energy dispersive X-ray diffraction; mean stress sensitivity; environmental sensitivity

1. Introduction

Ti-54M is a (α+β) titanium alloy which was developed by TIMET, Henderson, NV (USA) that can offer improved machinability (increased cutting speed and/or improved cutting tool life) as compared to the well known Ti-6Al-4V [1]. The alloy is produced through Electron Beam Single Melt Process (EBSM) as the alloy can take mix scrap such as Ti-6Al-4V and other alloys containing one of Mo, V and Fe. In addition to flexibility in raw material, it was found that machinability of Ti-54M was superior to Ti-6Al-4V [2]. Ti-54M will save machining cost in same parts that require extensive machining. While improvements in machinability over Ti-6Al-4V are well documented in the literature, there is lack in information to what extent mechanical surface treatments such as shot peening (SP) or ball-burnishing (BB) can improve the HCF performance of Ti-54M. In general, all mechanical surface treatments lead to surface strengthening by the induced high dislocation densities and residual compressive stresses [3, 4]. Residual compressive stresses are well known to enhance the fatigue performance and corrosion resistance by retarding or even suppressing micro-crack growth from the surface into the interior. Previous studies have shown that fatigue failure in mechanically surface treated titanium alloys within the low stress, high cycle regime is often associated with subsurface (quasi-vacuum) fatigue crack nucleation. This phenomenon may be related to the presence of process-induced tensile residual stresses necessarily present below the mechanically treated surface and required to

balance the outer process-induced residual compressive stresses [5-9]. The residual stresses induced by mechanical surface treatments have been measured by applying ED using synchrotron radiation (10 to 80 keV). ED using synchrotron radiation is a non-destructive method for measuring residual stress gradients in near-surface region. Synchrotron sources produce high energy photons that are more penetrating than a conventional X-ray method [10, 11]. The present study was undertaken to investigate the HCF response of Ti-54M to SP and BB. The HCF performance after mechanical surface treatments was correlated with both mean stress and environmental sensitivities (vacuum vs. air) of the fatigue strength of the electropolished references.

2. Experiments

Ti-54M was received as square (38 x 38 mm) bar stock in as-milled condition. Blanks 50 mm in length were β-annealed at 1010°C for 30 min followed by water-quenching (WQ). These blanks were unidirectionally rolled at 800°C with a total deformation degree of $\varphi = 1.4$. From the rolled plates, specimen blanks were taken in transverse direction (TD) and were heat treated to obtain a fully equiaxed microstructure by annealing at 800 °C for 1 hour followed by either water quenching (WQ) or air cooling (AC). All material was given a final heat treatment at 500 °C for 24 hours to age-harden the α-phase by Ti_3Al precipitates and the β- phase by fine secondary α precipitates. The thermomechanical treatment (TMT) utilized to produce a coarse grained EQ microstructure in Ti-6Al-4V is given in [12]. This coarse grained EQ microstructure of Ti-6Al-4V will be compared to the fine grained EQ microstructure in Ti-54M.

The phase analysis of the EQ microstructure in Ti-54M was determined using synchrotron radiation at DESY (beamline Harwi-II) with a fitted wavelength of 0.1269Å (97.7 keV) using the diffraction pattern of Zn powder. The distance between the sample and the area detector was 1500 mm.

Tensile tests were performed on both alloys using threaded cylindrical specimens having gage lengths and diameters of 25 and 5 mm, respectively. Young's moduli were measured with strain gauges attached to the gauge length of the specimens. Initial strain rates were 6.7 x 10-4 s^{-1}. HCF tests were performed on hour-glass shaped specimens either in rotating beam loading (R = -1, 4 mm minimum diameter) or in axial loading at R = -1 and R = 0.1 (3 mm minimum diameter) in air. In addition, some axial fatigue tests at R = -1 was performed in high vacuum ($p < 10^{-5}$ mbar). Before fatigue testing, the specimens were electrolytically polished (100 μm removal from the as-machined surface) to exclude any machining effects that could mask the results. This condition is denoted as EP. SP was performed using spherically conditioned cut wire (SCCW14) having an average shot size of 0.36 mm. Peening was done to full coverage at an Almen intensity of 0.20 mmA. BB was done using a conventional lathe and a hydrostatically driven tool with a hard metal ball of 6 mm in diameter. The burnishing pressure was kept at 300 bars.

Residual stress measurements were performed by ED using synchrotron radiation at BESSY-II in Berlin. The characteristic of the used beamline EDDI offers a white X-ray beam with an energy range of 10 to 80 keV. The primary beam cross-section was 0.5 x 0.5 mm^2; the angular divergence in the diffracted beam was restricted by a double slit system with apertures of 0.03 x 5 mm^2 to $\Delta\theta \leq 0.005°$. To achieve a high information depth which depends on the absorption of the material, a scattering angle $2\theta = 8°$ was chosen. ED gives

complete diffraction spectra for a fixed detector position. Any Bragg reflection was obtained by a different X-ray energy (wavelength) which means the signal of any reflection belongs to a different depth in the sample as schematically shown in Figure 1.

Due to the power restriction of 80 keV, residual stresses up to maximum depths of 100 μm could be measured. In order to measure stresses in deeper regions, 4 additional samples were prepared. Several layers of 100 to 150 μm were removed by EP to allow determining of the residual stress-depth distribution up to 800 μm. Residual stresses were evaluated by means of the $\sin^2\psi$ method in steps of $\Delta\psi = 4°$ up to 80°. The measured residual stress values were corrected using the equation which is described elsewhere [13]. A modified multi-wavelength approach [14] for any energy line $E_{(hkl)}$ gives an average penetration depth $\tau_{(hkl)}$ (Eq. 1).

$$\tau_{(hkl)} = (\tau_{(hkl)\,min} + \tau_{(hkl)\,max})/2 \qquad (1)$$

Where $\tau_{(hkl)min}$ and $\tau_{(hkl)max}$ are the minimum and the maximum penetration depths corresponding to the maximum and minimum tilting angles, respectively. The diffraction elastic constants of α-phase reflections were calculated by the Kroener-Model [15].

3. Results and Discussion

3.1 Microstructure and phase analysis

The EQ/WQ microstructures of both Ti-54M and Ti-6Al-4V are shown in Figure 2. Both microstructures are fully equiaxed with the equilibrium volume fraction of β-phase located at the triple-points of the α-grain boundaries. The equiaxed α-grain sizes in Ti-54M and Ti-6Al-4V amount to about 3 μm (Fig. 2a) and 20 μm (Fig.2b), respectively. This marked difference in grain size is caused by the different TMT used. The cooling rate being

varied from WQ to AC had no significant effect on the EQ microstructure in both Ti-6Al-4V and Ti-54M.

By using synchrotron radiation, the volume fractions of α and β phases in Ti-54M could be determined. The results were obtained after fitting with Maud as shown in Figure 3a. The Debye Scherrer ring (Fig. 3b) clearly shows the presence of crystallographic texture in this alloy. Therefore, sum diffraction spectra were used to improve the accuracy of the calculated values. Using this procedure, the volume fractions of the α and β phases were calculated to be 90 % and 10 %, respectively.

3.2 Tensile and fatigue properties

The tensile results, Table 1, confirm the insensitivity of the EQ microstructure to cooling rate in both alloys because no difference in yield stress, tensile strength or ductility was observed between conditions WQ and AC. The yield stress and UTS in Ti-54M are markedly higher than in Ti-6Al-4V. This is mainly due to the α-grain size in Ti-54M being much bigger than in Ti-6Al-4V. The fatigue performance of the EQ/WQ condition of both alloys is illustrated in Figure 4 where S-N curves from axial loading of electropolished references at R = -1 and R = 0.1 are plotted in terms of maximum stress. In addition, results from R = -1 tests in vacuum are plotted. Both alloys exhibit HCF strengths in vacuum markedly higher than in air, this effect presumably being related to detrimental hydrogen effects on the α-phase during fatigue testing in air [16]. Figure 4 also shows that the S-N curve at R = 0.1 in terms of maximum stress is located significantly above that at R = -1 for Ti-54M (Fig. 4a) indicating a normal mean stress sensitivity of the HCF strength of this alloy in air. On the contrary, the HCF strength in Ti-6Al-4V in terms of maximum stress is relatively unaffected by R-ratio (mean stress). This behaviour is known as the so-called

anomalous mean stress sensitivity (Fig. 4b). Presumably, the different respond of Ti-54M and Ti-6Al-4V to fatigue loading at low tensile mean stresses is related to differences in α grain size. Obviously, HCF crack nucleation in the coarse grained Ti-6Al-4V at low tensile mean stresses (R = 0.1) is much easier than in the fine grained Ti-54M.

3.3 Near-Surface Properties

The residual stress-depth distribution in Ti-54M after SP and BB is illustrated in Figure 5. Obviously, the maximum residual stress of -700 MPa after SP is significantly lower than after BB -825 MPa. Furthermore, the depths of maximum stresses are about 50 μm and 240 μm after SP and BB, respectively. The much greater penetration depth after BB can also be seen in Figure 6, where micro-hardness-depth profiles are plotted for both SP and BB.

3.4 Fatigue Performance after Mechanical Surface Treatments

The fatigue performance in rotating beam loading in air of both alloys is shown in Figure 7, comparing SP and BB conditions with the electropolished references. The HCF performance of EP Ti-54M is slightly improved by SP and much more by BB (Fig. 7a). The 10^7 cycles fatigue strength increases from 650 MPa (EP) to 675 MPa and 780MPa after SP and BB, respectively. The greater amount and penetration depths of residual compressive stresses after BB as opposed to SP are thought to be the reason for the more pronounced improvement of the HCF strength after BB (Fig. 7a). On the contrary, the HCF performance in Ti-6Al-4V decreased after mechanical surface treatments from 400 MPa (EP) to 350 MPa and 250 MPa after BB and SP, respectively (Fig. 7b).

Fatigue crack nucleation sites in Ti-54M after SP and BB of specimens tested in the HCF regime are illustrated in Figure 8. While fatigue cracks in EP always nucleated at the

specimen surface independent of stress amplitude and environment, subsurface fatigue crack nucleation was found after BB (Fig. 8a) and SP (Fig. 8b). The more pronounced improvement in Ti-54M of the HCF strength after BB as opposed to SP is related to the greater depth of the fatigue crack nucleation site of 400 μm compared to 200 μm underneath the surface (Fig. 8, compare Fig. 8a and b). Similar depths of HCF crack nucleation sites after BB and SP were also observed in Ti-6Al-4V [16]. Presumably, the occurrence of subsurface fatigue crack nucleation is directly related to the process-induced residual tensile stresses balancing the outer compressive stress field. Since subsurface cracks must nucleate under quasi-vacuum conditions, both the materials fatigue strength in vacuum and the tensile mean stress sensitivity of the fatigue strength need to be taken into account. The improvements in HCF performance of Ti-54M after SP and BB (Fig. 7a) can be derived from both the fatigue strength value in vacuum being markedly higher than in air and from the normal mean stress sensitivity of its fatigue strength (Fig. 4a). On the contrary, the very marked loss in HCF strengths after SP and BB of Ti-6Al-4V (Fig. 7b) can be explained by the anomalous mean stress sensitivity observed in this coarse grained equiaxed microstructure [16] because no marked differences were observed between Ti-54M and Ti-6Al-4V with regard to environmental sensitivity of the HCF strength (Fig. 4, compare Fig. 4a and 4b).

Conclusions

The presented results indicate that the mean stress sensitivity of the HCF strength in titanium alloys affects the material's response regarding HCF strength after mechanical surface treatments such as SP and BB. This is due to the fact that subsurface (quasi-

vacuum) fatigue cracking is caused by residual tensile stresses balancing the process-induced residual compressive outer stress fields. In case of normal mean stress sensitivities, the HCF strength relative to the EP reference is more or less improved as is shown on Ti-54M due to less influence of tensile mean stresses on HCF crack nucleation. However, in case of anomalous mean stress sensitivities, the HCF strength can even decrease after SP or BB. The latter result is explained by the marked influence of tensile mean stresses on HCF strength as observed in Ti-6Al-4V. Comparing results on Ti-54M and Ti-6Al-4V it is thought that the α-grain size is the main parameter in affecting mean stress sensitivity and thus the HCF response to SP and BB.

Acknowledgements

The authors would like to thank Dr. Yoji Kosaka of TIMET Company for providing the Ti-54M alloy. They also acknowledge financial support of the Deutsche Forschungsgemeinschaft (DFG) under projects WA 692/32-2 and BR 961/5-2.

References

[1] V. Venkatesh, Y. Kosaka, J. Fanning, S. Nyakana, in: Proc. of the 11th Int. World Conference on Titanium (JIMIC5), M. Niinomi, S. Akiyama, M. Ikeda, M. Hagiwara, K. Maruyama (Eds.), Kyoto, Japan, 2007, pp. 713-716.

[2] S. L Nyakana, J. C Fanning, D. W. Tripp, in: Proc. of the 11th Int. World Conference on Titanium (JIMIC5), M. Niinomi, S. Akiyama, M. Ikeda, M. Hagiwara, K. Maruyama (Eds.), Kyoto, Japan, 2007, pp. 749-752.

[3] J. O. Almen, P. H. Black, Residual stresses and fatigue in met., McGraw-Hill, New York, 1963.

[4] V. Schulze, in: Proc. of the 8th Int. Conference on Shot Peening, L. Wagner (Eds.), Garmisch-Partenkirchen, Germany, 2002, pp. 145.

[5] E. Maawad, H.-G. Brokmeier, M. Hofmann, Ch. Genzel, L. Wagner, Mater. Sci. Eng. A 527 (2010) 5745–5749.

[6] E. Maawad, S. Yi, H.-G. Brokmeier, L. Wagner, in: Proc. of the 10th Int. Conference on Shot Peening, K. Tosha (Eds.), Tokyo, Japan, 2008, pp. 499-504.

[7] L. Wagner, M. Wollmann, in: Proc. of the 10th Int. Conference on Shot Peening, K. Tosha (Eds.), Tokyo, Japan, 2008, pp. 355-362.
[8] T. Ludian, M. Kocan, H. J. Rack, L. Wagner, J. Mater. Res. 97 (2006) 1425-1431.
[9] L. Wagner, Mater. Sci. Eng. A263 (1999) 210–216.
[10] T. Kuntz, H. Wadley, D. Black, Metall. Trans. A 24A (1993) 1117.
[11] A. Pyzalla, J. Nondestructive Evaluation 19 (2000) 21.
[12] J. Mueller, H. J. Rack, L. Wagner, in: Proc. of the 11th Int. World Conference on Titanium (JIMIC5), M. Niinomi, S. Akiyama, M. Ikeda, M. Hagiwara, K. Maruyama (Eds.), Kyoto, Japan, 2007, pp. 383-386.
[13] M.G. Moore, W.P. Evans, SAE Trans., 66 (1958) 340-345.
[14] Ch. Genzel, C. Stock, B. Wallis and W. Reimers: J. Nucl. Instrum. Methods A 467-468
(2001) 1253-1256.
[15] E. Kroener, Z. Phys. 151 (1958) 504-518.
[16] M. Kocan, H. J. Rack and L. Wagner, in: Proc. of the 11th Int. World Conference on Titanium (JIMIC5), M. Niinomi, S. Akiyama, M. Ikeda, M. Hagiwara, K. Maruyama (Eds.), Kyoto, Japan, 2007, pp. 1241-1244.

Figure Captions

Figure 1: Scheme showing relation between energy (E) and penetration depth (τ) of white X-ray beam.
Figure 2: Equiaxed microstructures of (a) Ti-54M EQ/WQ and (b) Ti-6Al-4V EQ/WQ.
Figure 3: (a) Sum diffraction pattern of Ti-54M (EQ) fitted by Maud and (b) Debye-Scherrer ring.
Figure 4: S-N curves of both alloys: Effect of R-ratio and environment on (a) Ti-54M EQ/WQ and (b) Ti-6Al-4V EQ/WQ.
Figure 5: Residual stress-depth profiles in Ti-54M.
Figure 6: Micro-hardness-depth profiles in Ti-54M.
Figure 7: S-N curves (R = -1), Effect of shot peening and ball burnishing (rotation beam loading) on (a) Ti-54M and (b) Ti-6Al-4V.
Figure 8: HCF crack nucleation sites in EQ/WQ microstructures of Ti-54M after (a) BB and (b) SP.

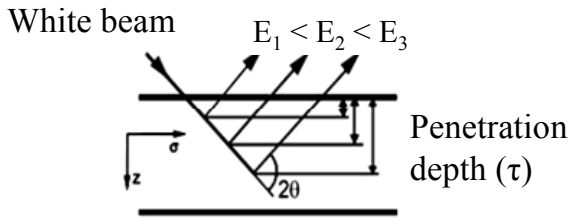

Figure 1: Scheme showing relation between energy (E) and penetration depth (τ) of white X- ray beam.

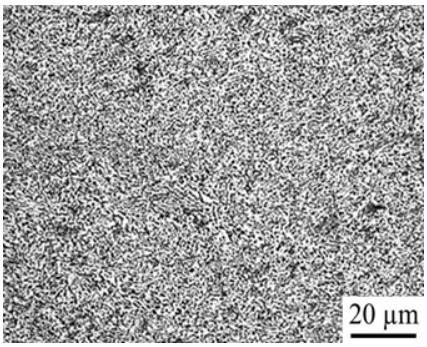

(a)

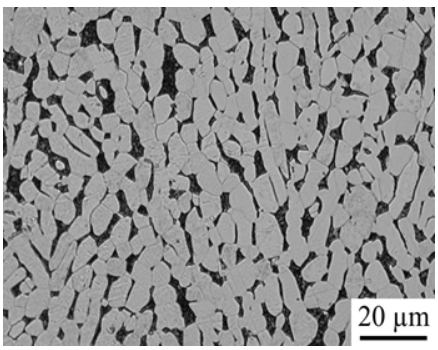

(b)

Figure 2: Equiaxed microstructures of (a) Ti-54M EQ/WQ and (b) Ti-6Al-4V EQ/WQ.

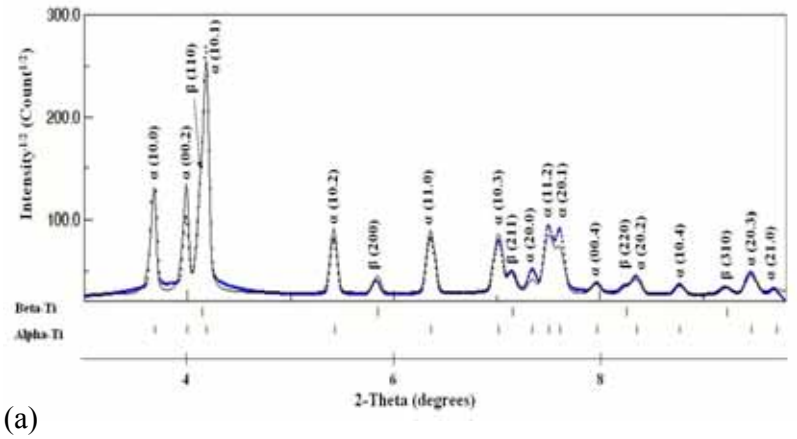

(a)

(b)

Figure 3: (a) Sum diffraction pattern of Ti-54M (EQ) fitted by Maud and (b) Debye-Scherrer ring.

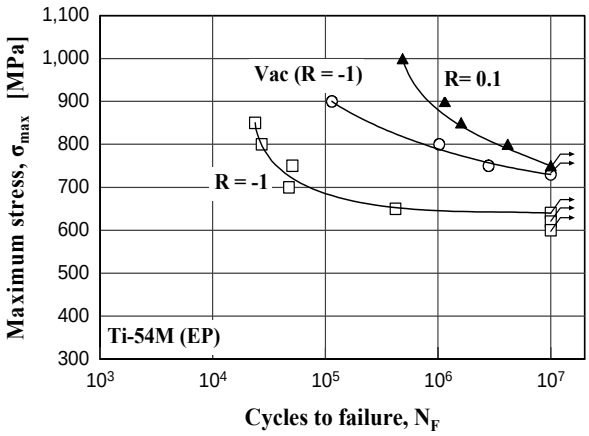

(a)

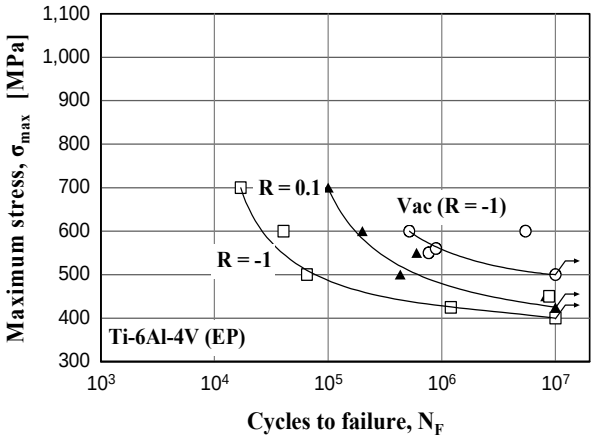

(b)

Figure 4: S-N curves of both alloys: Effect of R-ratio and environment on (a) Ti-54M EQ/WQ and (b) Ti-6Al-4V EQ/WQ.

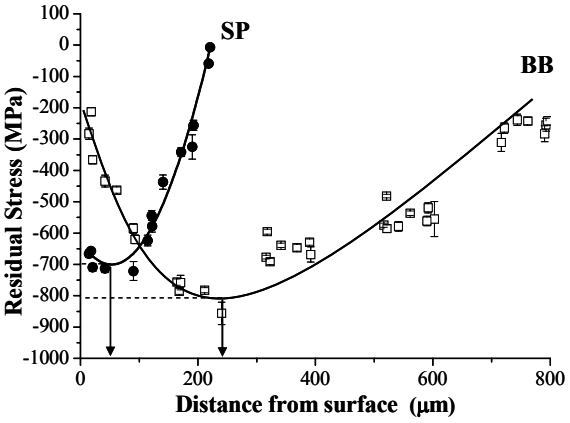

Figure 5: Residual stress-depth profiles in Ti-54M.

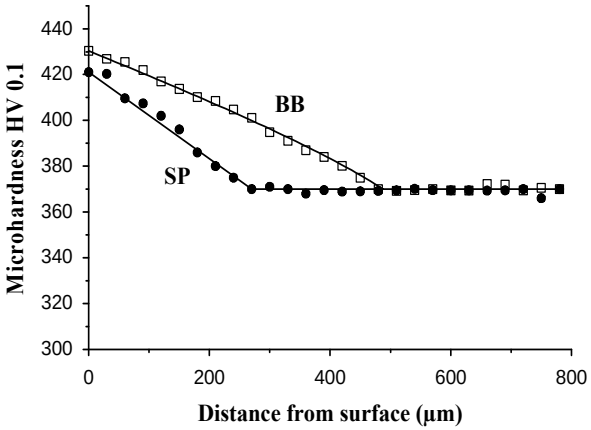

Figure 6: Micro-hardness-depth profiles in Ti-54M.

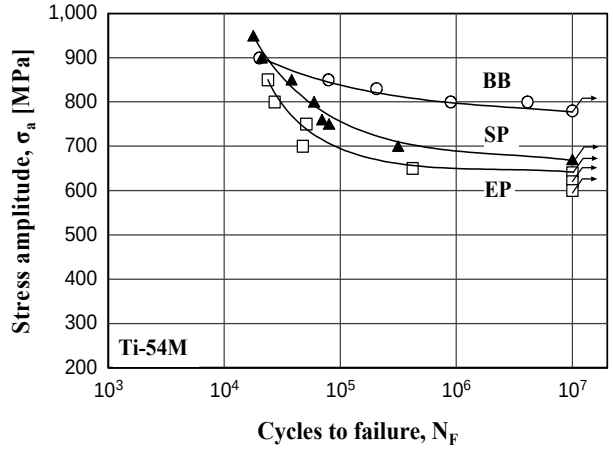

(a)

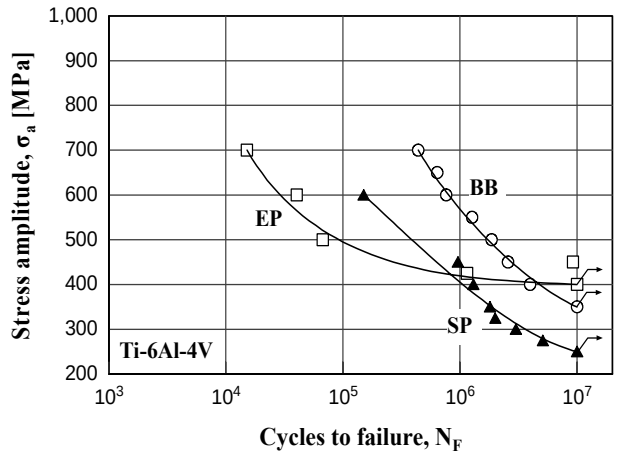

(b)

Figure 7: S-N curves (R = -1), Effect of shot peening and ball burnishing (rotation beam loading) on (a) Ti-54M and (b) Ti-6Al-4V.

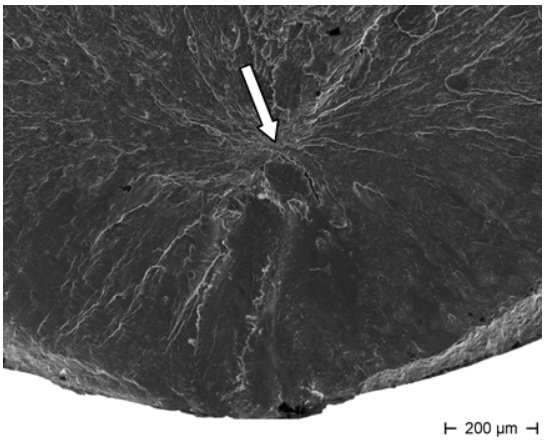

(a)

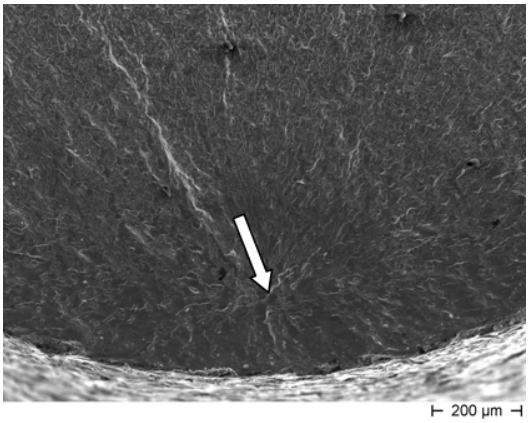

(b)

Figure 8: HCF crack nucleation sites in EQ/WQ microstructures of Ti-54M after (a) BB and (b) SP.

Table 1: Tensile properties of EQ microstructures of both alloys: Effect of cooling rate

Microstructure	Cooling	$\sigma_{0.2}$ (MPa)	UTS (MPa)	El (%)	$\varepsilon_F = \ln (A_o/A_F)$
Ti-54M	WQ	1145	1145	12.6	0.62
	AC	1135	1145	15.5	0.72
Ti-6Al-4V	WQ	1045	1075	15.6	0.35
	AC	1045	1075	15.8	0.30